physica status solidi

pss

www.pss-journals.com

reprint

WILEY-VCH

Phys. Status Solidi A **212,** No. 3, 623–631 (2015) / **DOI** 10.1002/pssa.201431556

physica status solidi a
www.pss-a.com
applications and materials science

Enhanced low-field magnetoresistance of $La_{0.7}Sr_{0.3}Mn_{1-x}Ni_xO_3$ compounds by annealing process

A. M. Ahmed, M. A. Abedellateef, H. A. Abd El-Ghanny, and Abd El Mo'ez A. Mohamed*

Physics Department, Faculty of Science, Sohag University, 82524 Sohag, Egypt

Received 3 August 2014, revised 13 September 2014, accepted 22 September 2014
Published online 28 October 2014

Keywords electrical properties, magnetoresistance, manganites, thermoelectric properties

* Corresponding author: e-mail abdmoez_hussien@science.sohag.edu.eg, Phone: +20934602964, Fax: +20934601159

A study of Mn-site substitution by Ni^{2+} and the effect of annealing time in polycrystalline bulk $La_{0.7}Sr_{0.3}MnO_3$ in composition range ($0 \le x \le 0.1$) is presented. This study involves structural, electrical, magnetoresistance, and thermoelectric power (TEP) measurements. X-ray diffraction was used to examine the structure for the as-prepared and annealed samples, and it shows that there is no change in structure with annealing time. Electrical resistivity and magnetoresistance are strongly affected by annealing process, where there is a dramatic increase in resistivity with annealing time and an enhancement in magnetoresistance in different temperature ranges. Moreover, conduction mechanisms above and below transition temperature (T_{ms}) are discussed, since, variable-range hopping and small-polaron hopping models are applied above T_{ms}, in addition to some experimental relations below it. In addition, the TEP sign changes from positive to negative with doping and annealing.

1 Introduction Perovskite colossal magnetoresistive manganites have been studied carefully since their wonderful properties began to be known such as electrical resistivity (ρ) transition from metal to semiconductor behavior at a certain temperature T_{ms} and ρ suppression under magnetic-field application and hence the so-called magnetoresistance (MR). The structural and the electronic configuration of these materials play a crucial role in its properties explanation as Mn^{4+} and Mn^{3+} valence exchange [1], charge localization through Jahn–Teller effect [2] and oxygen vacancies. The importance of these materials is related to MR phenomenon applications, such as magnetic sensors and magnetic data storage devices [3]. This property made them good potential application materials [4] and especially the La–Sr–Mn–O system that became a reference [5], where the Sr^{2+} system is known with its room temperature T_{ms} [6]. The high values of MR are obtained under high magnetic fields, which hinder its potential applications, while polycrystalline or granular material tends to show high MR values under low magnetic fields, which known as low-field magnetoresistance all over temperature ranges due to the presence of grain boundaries [7]. In another way, these oxides were found to be good thermoelectrics [8], and this discovery draws attention in this direction [9, 10]. The importance of thermoelectric power (TEP) is not only related to applications, but also to understand the transport mechanism in polycrystalline materials [11].

Ni^{2+} was substituted previously in Mn sites in several systems such as in (La, Ca)MnO_3 [12, 13] and (La, Sr) MnO_3 [14–16] and it was found to alter transport, magnetic and sometimes structural properties by changing the Mn^{3+}/Mn^{4+} ratio. But, annealing-effect studies in this transition metal have not received enough attention. So, in this work, we will investigate the effect of annealing time on $La_{0.7}Sr_{0.3}Mn_{1-x}Ni_xO_3$ compounds, trying to determine its effect on transport properties that may have an important effect on these properties of perovskite materials [17] seeking to obtain an enhancement in MR given by these compounds.

2 Experimental $La_{0.7}Sr_{0.3}Mn_{1-x}Ni_xO_3$ series compositions with $x = 0$, 0.075, and 0.1 at.% were prepared by the conventional solid-state reaction method. High purity powders of La_2O_3, $SrCO_3$, $MnCO_3$, and NiO were mixed in stoichiometric proportions. La_2O_3 was dehydrated at 873 K for 6 h. The mixture was ground for 6 h to ensure

homogeneity, pelletized and calcined in air at 1173 K for 10 h. Then, they were reground for 5 h, pelletized, sintered at 1373 K for 20 h and left for gradual cooling to room temperature. Samples were exposed to an annealing process for 10 and 20 h at 1173 K. The electrical measurements were carried out by the standard four-point Van der Pauw technique in the temperature range 80–290 K [18–20], and under a magnetic field of 0.5 T. Samples were examined by X-rays, using a Brucker (Axs-D& Advace) powder diffractometer at room temperature with CuKα radiation ($\lambda = 1.5406$ Å) and the microstructure was investigated by a Jeol JSM-6610LV scanning electron microscope (SEM).

3 Results and discussion

3.1 Structure Figure 1 shows XRD patterns of the as-prepared and annealed polycrystalline $La_{0.7}Sr_{0.3}Mn_{1-x}Ni_xO_3$ ($x = 0$, 0.075, and 0.1 at.%) samples. These patterns show that they are nearly single phase with a small La_2O_3 impurity peak around $2\theta = 30^\circ$ whose intensity decreases with doping, the same peak was previously observed by other researchers [21]. Rietveld refinement for the XRD patterns proved the crystallization of parent compound LSMO in the R-3c rhombohedral structure and doped samples in the Pbnm orthorhombic structure. There is no change in structure with annealing times compared with the as-prepared samples, where LSMO is still rhombohedral and doped samples are still orthorhombic, just a slight tendency to decrease in peak intensity. This stability in structure and intensity decrease with annealing time was observed and reported also by [22]. In addition, there are no new peaks, that means there are no additional phases. Particle size was calculated from XRD using the Laue–Scherrer equation, it decreases with doping and with annealing times as listed in Table 1, that will have an important effect on the related transport properties as will be seen later.

To check the presence of elements in $La_{0.7}Sr_{0.3}Mn_{1-x}Ni_xO_3$, energy-dispersive analysis by X-rays (EDAX) was carried out, and Fig. 2 shows the existence of every element in the as-prepared and annealed samples. Sample morphology was determined using SEM that was carried out on the powder compounds of as-prepared and 20 h annealed samples. As in Fig. 3, SEM micrographs for samples show that both Ni^{2+} doping and annealing process reduce grain size, and the grains agglomerate with each other forming clusters. This behavior may be explained by considering the grain boundary effects. Also, it is noted that the SEM average grain size is greater than the XRD particle size (Table 1) that indicates grain may contain several particles [23].

3.2 Electrical properties Figure 4 shows the temperature dependence of resistivity curves, $\rho(T)$, for the as-prepared and annealed samples. For the as-prepared samples, there is a decrease in T_{ms} (Table 2) towards lower temperatures with doping disappears at $x = 0.1$ and an increase in resistivity, that is in agreement with [16]. The as-prepared LSMO has a small T_{ms} compared with previous works that may be attributed to the smaller particle and

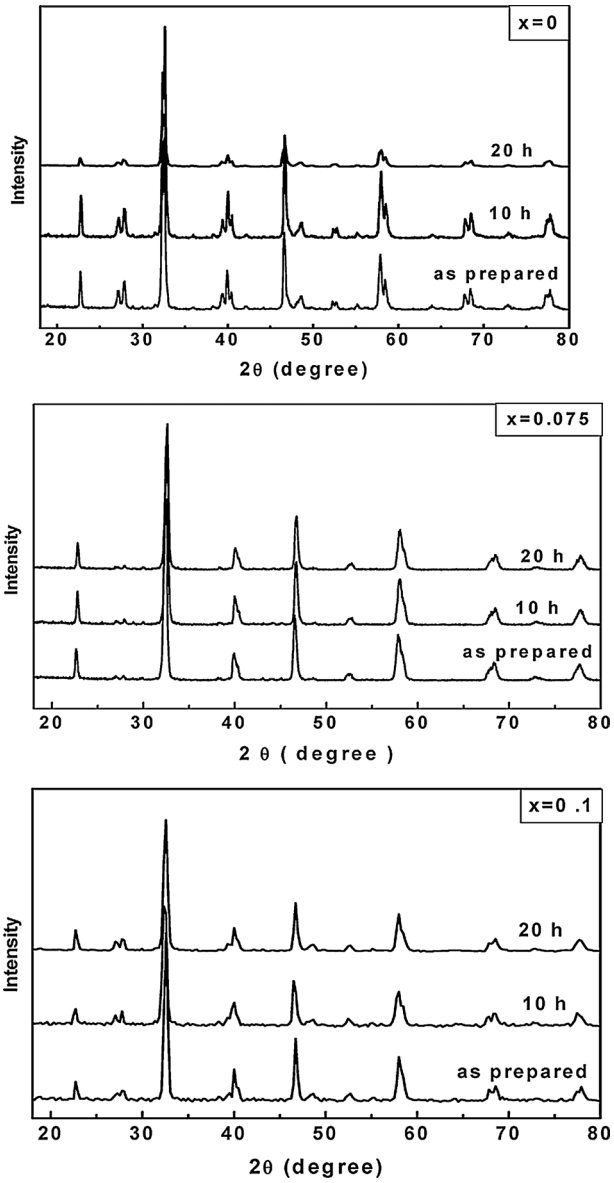

Figure 1 XRD patterns of the as-prepared and annealed samples of $La_{0.7}Sr_{0.3}Mn_{1-x}Ni_xO_3$ ($x = 0$, 0.075, and 0.1).

Table 1 Grain size and particle size calculated from SEM and XRD, respectively.

x	conditions	SEM (μm)	particle size (nm)
0	as-prepared	0.752	23.52
	10 h	–	23.4
	20 h	0.573	16.56
0.075	as-prepared	0.582	16.85
	10 h	–	16.54
	20 h	0.379	16.31
0.1	as-prepared	0.394	16.34
	10 h	–	13.6
	20 h	0.313	13

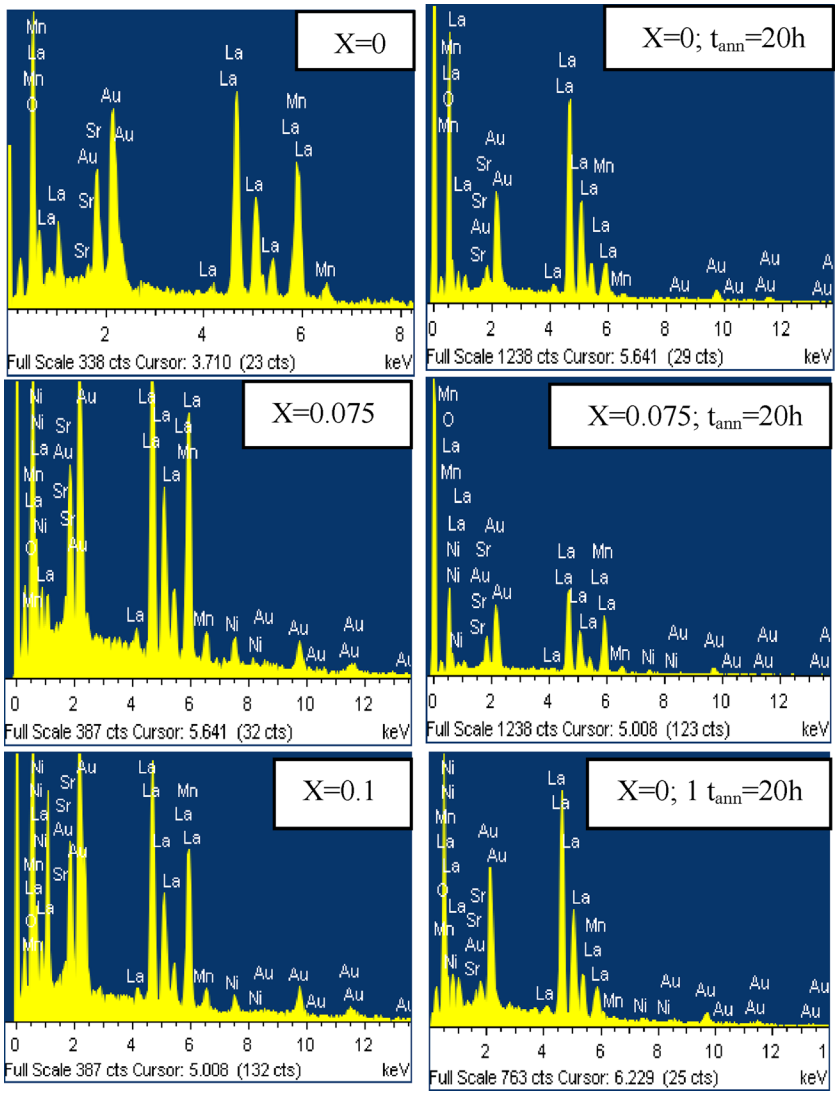

Figure 2 Energy-dispersive analysis by X-rays (EDAX) of the as-prepared and 20 h annealed samples.

grain size [24]. Also, with increasing annealing time, we can see the same behavior in T_{ms} and ρ. These two important conjugated phenomena, T_{ms} decrease and resistivity increase, may be due to some correlated transport and structural reasons, as double-exchange mechanism (DE) decreases because of the disturbance in Mn^{3+}/Mn^{4+} ratio, oxygen-vacancy introduction [25], particle and grain size decrease (Table 1) and MnO_6 tilting distortion that increases as a result of Mn substitution by Ni^{2+} ions, that helps Mn–O–Mn bond bending. In the as-prepared samples, Ni^{2+} content increase is responsible for the DE decrease, while in the annealed samples, the DE decrease is related to the decrease in Mn^{4+} ratio that can be affected by heat treatment [26] due to oxygen vacancies formation [25] and hence the increased resistivity, that was previously observed by [27] in annealed $La_{0.67}Ca_{0.33}MnO_3$. With respect to the structural reasons, decreasing Mn^{4+} by the annealing process increases Mn^{3+} ratio, which is a Jahn–Teller active ion, so there is an increase in distortion that increases resistivity. Also, grain size plays an important role in the transport properties, as stated above. From Table 1, grain size decreases with doping and annealing time, that is in agreement with [28], this decrease results in various consequences. First, grain size decrease can decrease bond angle and increase its length [29]. Secondly, the grain's outer shell ratio or surface ratio increases with decreasing grain size [30], and this layer has random magnetic states and defects [31, 32]. Both of the previous consequences can decrease DE, increase resistivity and decrease T_{ms} with doping and annealing time.

3.3 Magnetoresistance (MR) Figure 5 shows the temperature dependence of MR of the as-prepared and annealed samples. This figure exhibits the significance of the annealing process on MR. In the LSMO parent sample, the first annealing time (10 h) increases the MR peak height around 155 K from −9% to −28.11%, and the second annealing time (20 h) increases it with more height to −34.58% with a shift to 150 K. With respect to room

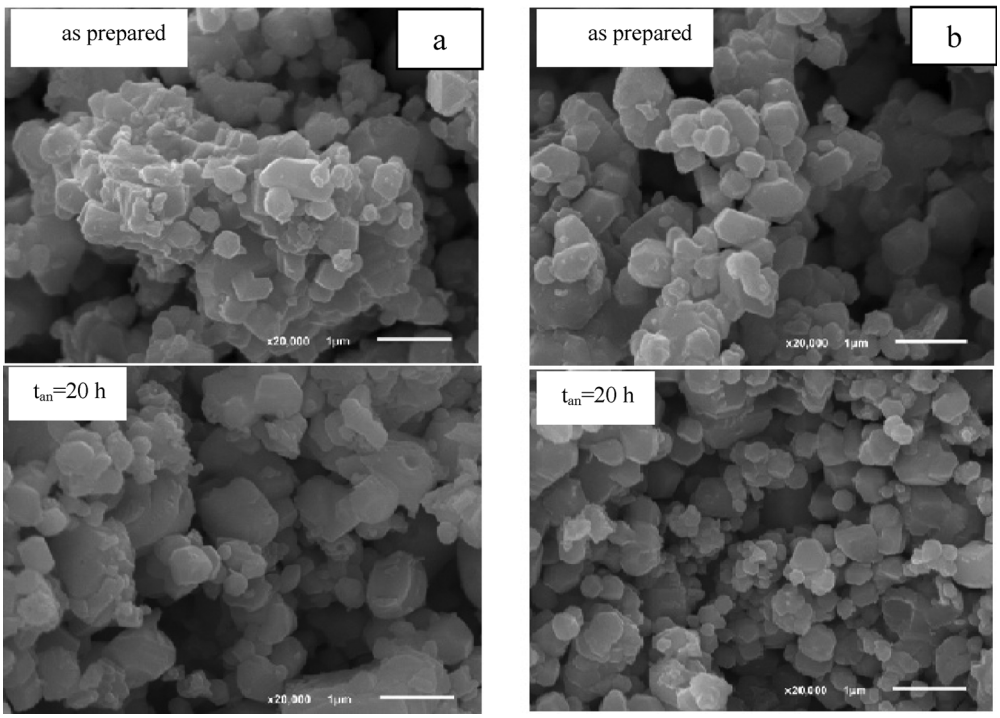

Figure 3 SEM micrographs of as-prepared and annealing for 20 h samples $x = 0$ (a) and $x = 0.075$ (b).

temperature (RT) (290 K) MR, an enhancement from −0.13% to −4.59% and −2.37% is observed for 0, 10 h, and 20 h annealing times, respectively. The MR of $x = 0.075$ is notably enhanced in RT, where it increases from −0.73% to −8.45% and −10% upon annealing at 10 and 20 h, respectively. On the other hand, the as-prepared $x = 0.1$ exhibits a broad peak around 200 K, and is shifted to higher temperatures around 225 K with the first annealing time (10 h), nearly with the same MR value. With 20 h annealing time, this peak becomes sharper and is shifted to 155 K with MR height −11.94%, this reveals an enhancement in MR at this temperature compared with the as-prepared one. The enhancement in MR for all samples with annealing times in different temperature ranges may be ascribed to oxygen deficiency [33] and grain boundaries due to grain size decrease or spin-dependent scattering at these grain boundaries [7] that is due to spin-polarized carriers tunneling across barriers.

3.4 Conduction mechanism above and below T_{ms} To know the nature of conduction, the parts of $\rho(T)$ curves above and below T_{ms} will be studied independently. In the semiconducting region (above T_{ms}), various investigations have discussed the presence of two important main conduction mechanisms, small polaron hopping (SPH) and Variable-range hopping [3, 34]. Figure 6a shows data fitting of the as-prepared $x = 0.075$ as an example with SPH model of Mott and Davis [35] with expression $\rho/T = \rho_0 \exp(E\rho/k_BT)$ at $T > \theta_D/2$ [35], where $\rho_0 = [k_B/\upsilon_{ph}Ne^2R^2C \times (1-C)\exp(2\alpha R)]$, k_B is Boltzmann constant, T is the absolute temperature, N is the number of ion sites per unit volume, $R \sim (1/N)^{1/3}$ is the average intersite spacing, C is the fraction of sites occupied by a polaron, α is the electron wave function decay constant, υ_{ph} is the optical phonon frequency (estimated from $h\upsilon_{ph} = k_B\theta_D$ relation, θ_D is Debye temperature) and $E\rho$ is the sum of the activating energy and the energy required to create free carriers (disorder energy). $E\rho$ can be written as

$$E\rho = W_H + W_D/2 \quad \text{for } T > \theta_D/2, \tag{1}$$

$$= W_D \quad \text{for } T < \theta_D/4, \tag{2}$$

where W_D is the disorder energy and W_H is the polaron hopping energy, W_H is the difference between the electric and thermopower activation energies ($W_H = E_p - E_s$) [36].

Heat treatment of the parent LSMO decreases θ_D (K) and υ_{ph} (Hz) with annealing times (Table 2), which means an increase in the SPH range, while a decrease in the SPH range in the doped samples is noticed, which causes an increase in the same parameters upon annealing time. The $E\rho$ and W_H parameters increase with increasing doping and annealing times as is clear from Tables 2 and 4. This increase in $E\rho$ may be due to the increase in e_g electron localization that results from electron–phonon interaction (γ_{ph}), that results in a decrease in the number of states $N(E_f)$ (Table 4), and so an increase in resistivity. It can be emphasized by the non-sequence increase in γ_{ph} (Table 3) that has been estimated for the as-prepared and annealed samples and has the same strong electron–phonon interaction since it is

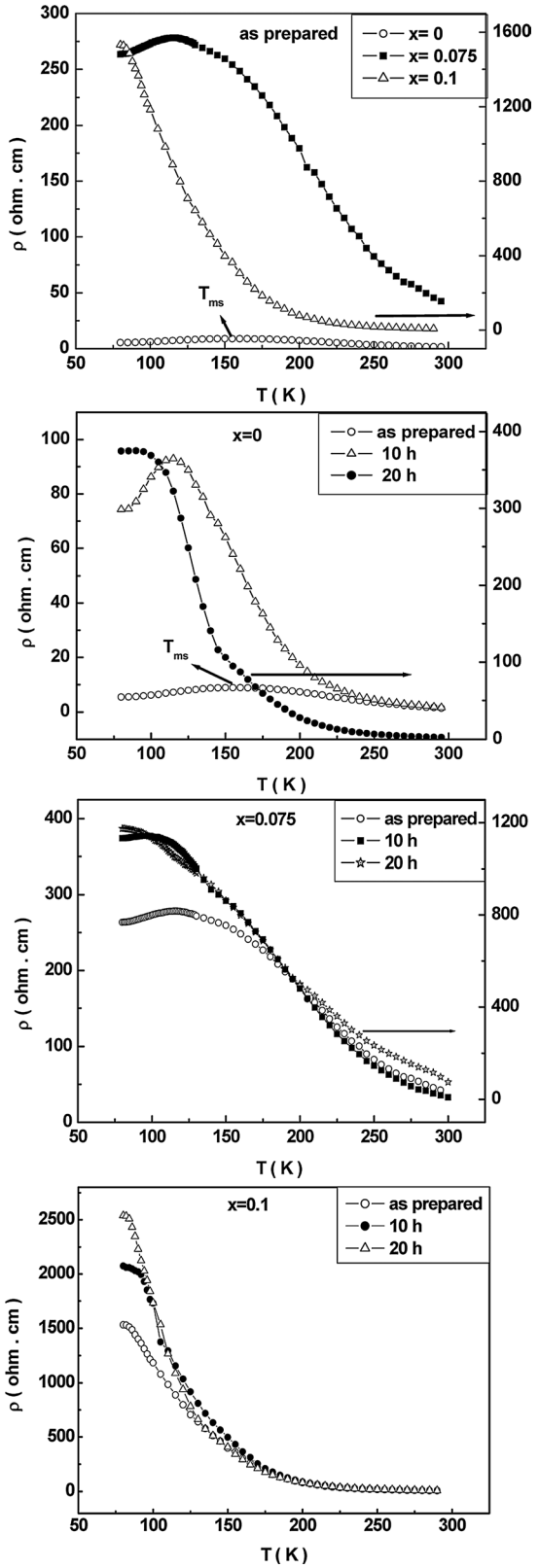

Figure 4 Temperature dependence of resistivity for the as-prepared and annealed samples of $La_{0.7}Sr_{0.3}Mn_{1-x}Ni_xO_3$ ($x = 0$, 0.075, and 0.1).

Table 2 T_{ms}, $E\rho$, θ_D and υ_{ph} determined for the as-prepared and annealed samples of $La_{0.7}Sr_{0.3}Mn_{1-x}Ni_xO_3$.

x	conditions	T_{ms} (K)	$E\rho$ (meV)	θ_D (K)	υ_{ph} (Hz)
0	as-prepared	155	111.23	430	8.96×10^{12}
	10 h	115	140.45	370	7.71×10^{12}
	20 h	90	143.33	360	7.5×10^{12}
0.075	as-prepared	116	112.60	440	9.17×10^{12}
	10 h	94	115.75	440.04	9.17×10^{12}
	20 h	–	117.71	460	9.59×10^{12}
0.1	as-prepared	–	127.94	349.9	7.29×10^{12}
	10 h	–	147.91	350	7.3×10^{12}
	20 h	–	150.94	370.37	7.72×10^{12}

still greater than 4 ($\gamma_{ph} > 4$) [37]. Grain size also can be a reason contributing to the $E\rho$ increase. As a result of the grain size decrease or increasing in grain boundaries with annealing times, the spins in the outer shell of the grain will be more random, according to the core–shell model [30]. This may give rise to the probability of Mn^{3+}, Mn^{4+}, and Ni^{2+} to not having the same spin alignment, which makes polaron hopping between these ions more difficult and needs more energy for hopping [38].

Results in Table 3 confirm small-polaron formation even in the annealing conditions for both parent and doped samples, because they still obey the relation $J < W_H/3$, which is the condition of small-polaron formation [39]. To determine what happens if the conduction by small polaron is adiabatic or nonadiabatic, Holstein criteria are applied [39], where:

$J > H$ for adiabatic condition,
$J < H$ for nonadiabatic condition,

where

$$J(T) \approx 0.67\, h\upsilon_{ph}\, (T/\theta_D)^{1/4}, \tag{3}$$

and

$$H = (2k_B T W_H/\pi)^{1/4}\, (h\upsilon_{ph}/\pi)^{1/2}. \tag{4}$$

According to these criteria, Table 3 shows that the as-prepared samples $x = 0$ and 0.075 are in the adiabatic conduction state ($J > H$), and $x = 0.1$ is in the nonadiabatic one, while, in heat treatment, with increasing annealing times, the parent compound cannot preserve the adiabatic conduction of its as-prepared system and converts to the nonadiabatic system, verifying the condition J (290 K) $< H$ (290 K) for all annealing times. Heat treatment of doped samples cannot affect their as-prepared conduction state, where $x = 0.075$ still in the adiabatic conduction state and $x = 0.1$ in the nonadiabatic conduction state for all annealing times.

With respect to the VRH model that has the formula $\sigma = \sigma_0 \exp(-T_0/T)^{1/4}$ [35], Fig. 6b shows the best fitting with

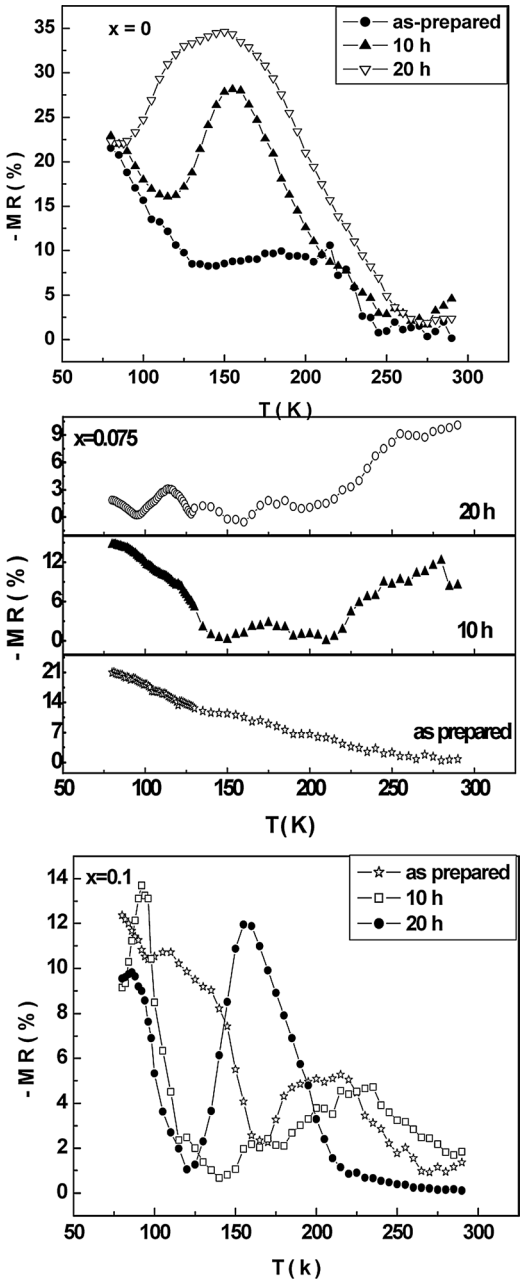

Figure 5 Temperature dependence of magnetoresistance for the as-prepared and the annealed samples of $La_{0.7}Sr_{0.3}Mn_{1-x}Ni_xO_3$ ($x = 0$, 0.075, and 0.1).

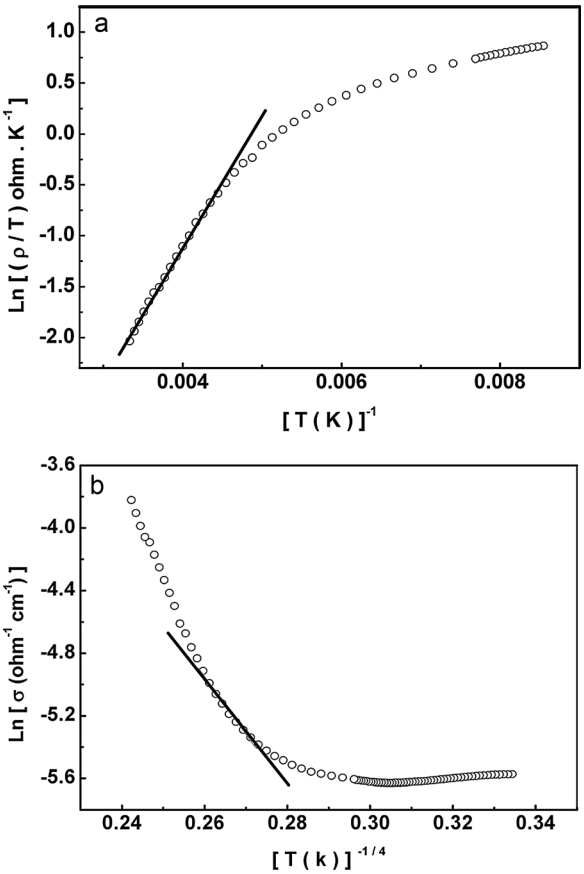

Figure 6 (a) SPH and (b) VRH models for the as-prepared $x = 0.075$, where the straight line represents the best-fitted points with these models.

this model in temperature range $T_{ms} < T < \theta_D/2$. In this concept, carriers can hop from one site to another and this needs energy, so it was important to determine some related parameters such as hopping energy (E_h) and hopping distance (R_h). These parameters were determined at 290 K from the relations $E_h(T) = 1/4k_BT^{3/4}T_0^{1/4}$ and $R = 3/8a \times (T_0/T)^{1/4}$, respectively [40]. Due to e_g electron localization and Mn–O–Mn angle decreasing with annealing time, carriers need more energy for hopping. So, we can see an increase in E_h, R_h and a decrease in $N(E_f)$ (Table 4) that may appear as an increase in the resistivity.

At low temperatures, below T_{ms}, the following empirical equations were applied to the electrical resistivity data:

$$\rho = \rho_0 + \rho_2 T^2, \quad (5)$$

$$\rho = \rho_0 + \rho_{2.5} T^{2.5}, \quad (6)$$

Table 3 H, J, $W_H/3$, and γ_{ph} parameters determined for the as-prepared and annealed samples.

x	conditions	H (meV)	J (meV)	$W_H/3$	γ_{ph}
0	as-prepared	22.21	22.45	36.73	5.96
	10 h	21.86	20.05	46.57	8.78
	20 h	21.65	19.64	47.31	9.17
0.075	as-prepared	22.45	22.48	36.6	5.8
	10 h	22.62	22.84	37.74	5.98
	20 h	22.6	23.61	34	5.21
0.1	as-prepared	20.73	19.23	42.13	8.39
	10 h	21.47	19.24	48.35	9.63
	20 h	22.19	20.07	49.36	9.3

Table 4 $N(E_F)$, W_H, R_h, and E_h determined for as-prepared and annealed samples.

x	conditions	$N(E_F)$ ($eV^{-1}\,cm^{-3}$)	W_H (meV)	R_h (Å)	$E_h(T)$ (meV)
0	as-prepared	47.51×10^{20}	110.19	10.77	39.92
	10 h	34.16×10^{20}	139.71	11.7	43.35
	20 h	2.39×10^{20}	141.94	22.73	84.23
0.075	as-prepared	12.57×10^{20}	109.81	15	55.59
	10 h	12.3×10^{20}	113.23	15.08	55.91
	20 h	11.8×10^{20}	103	15.26	56.55
0.1	as-prepared	10.8×10^{20}	126.39	15.57	57.72
	10 h	9.3×10^{20}	145.06	16.27	60.30
	20 h	3.68×10^{20}	148.09	20.41	75.66

Table 5 The square of linear correlation coefficient (R^2) values in the ferromagnetic region for the as-prepared and annealed samples.

x	conditions	Eq. (5)	Eq. (6)	Eq. (7)	Eq. (8)
0	as-prepared	0.987	0.981	0.991	0.999
	10 h	0.981	0.983	0.990	0.999
	20 h	0.970	0.970	0.987	0.990
0.075	as-prepared	0.963	0.959	0.997	0.999
	10 h	0.990	0.989	0.990	0.996
	20 h	–	–	–	–
0.1	as-prepared	–	–	–	–
	10 h	–	–	–	–
	20 h	–	–	–	–

$$\rho = \rho_0 + \rho_2 T^2 + \rho_{4.5} T^{4.5}, \tag{7}$$

$$\rho = \rho_0 + \rho_2 T^2 + \rho_{4.5} T^{4.5} + \rho_5 T^5. \tag{8}$$

Equation (8) was found to be the best-satisfied one (Table 5), which confirms the presence of grain boundaries (ρ_0), electron–electron ($\rho_2 T^2$), electron–phonon interactions ($\rho_5 T^5$), and spin-wave fluctuation ($\rho_{4.5} T^{4.5}$). From Table 6, a general increase in ρ_0, ρ_2, $\rho_{4.5}$, and ρ_5 with annealing time for both parent LSMO and $x = 0.075$ can be seen, but the grain-boundary component ρ_0 is the most effective one.

3.5 Thermoelectric power Thermoelectric power investigation was carried out in terms of Seebeck coefficient (S) variation with temperature, and the annealing process had a notable effect on the thermoelectric properties. The S values of as-prepared and annealed samples are in microvolts, and exhibit a crossover from positive to negative sign at a certain temperature T^* for the as-prepared $x = 0$ and 0.075 samples. T^* decreases with increasing annealing time as shown in Table 7, which means a decrease in hole conduction interval or an enhancement in electron conduction dominance with annealing times. Figure 7 shows the temperature dependence of S, $S(T)$, and we can see a non-sequential increase towards negative S with annealing time. This can be attributed to the influence of Mn^{4+} ions by annealing process [41] and oxygen vacancies, which results in a decrease in its ratio compared with Mn^{3+}, and may be the reason for the increase of S at high temperatures [42]. Also, with looking at the room temperature S, we can see a general improvement in its absolute value with annealing time.

Table 7 E_s, α and T^* determined from TEP above T_s value.

x	conditions	E_s (meV)	$(e/k_B)\alpha$	T^* (K)
0	as-prepared	1.039	−8.5	148
	10 h	0.74	−11.1	–
	20 h	1.39	−9.8	–
0.075	as-prepared	2.78	−1.9	233
	10 h	2.51	−11.3	163
	20 h	14.47	−58.71	143
0.1	as-prepared	1.54	−10.4	108
	10 h	2.84	−9.48	–
	20 h	1.62	−11.3	–

In addition, the $S(T)$ curves exhibit a slightly broad peak at T_s, and here, we will try to analyze regions above and below T_s. In ferromagnetic materials, there are spin interactions with electrons that cause magnon drag and interaction between electrons and phonons producing phonon drag. The $S(T)$ variation below T_s was analyzed by the equation

$$S = S_0 + S_1 T + S_{3/2} T^{3/2} + S_3 T^3 + S_4 T^4, \tag{9}$$

where S_0 is a constant, S_1 is the diffusion coefficient, $S_{3/2}$ is the magnon drag coefficient, S_3 is the phonon drag

Table 6 Best-fit parameters obtained from experimental resistivity data in the ferromagnetic metallic region.

x	conditions	ρ_0	ρ_2	$\rho_{4.5}$	ρ_5
0	as-prepared	6.23	479×10^{-4}	1.5×10^{-1}	1.1×10^{-9}
	10 h	181.1	3.99×10^{-2}	1.2×10^{-6}	9.6×10^{-8}
	20 h	347	5.04×10^{-4}	5.4×10^{-7}	5.3×10^{-8}
0.075	as-prepared	265.2	57×10^{-4}	31.2×10^{-8}	24×10^{-9}
	10 h	484.1	4.6×10^{-2}	1.8×10^{-6}	1.4×10^{-7}
	20 h	–	–	–	–
0.1	as-prepared	–	–	–	–
	10 h	–	–	–	–
	20 h	–	–	–	–

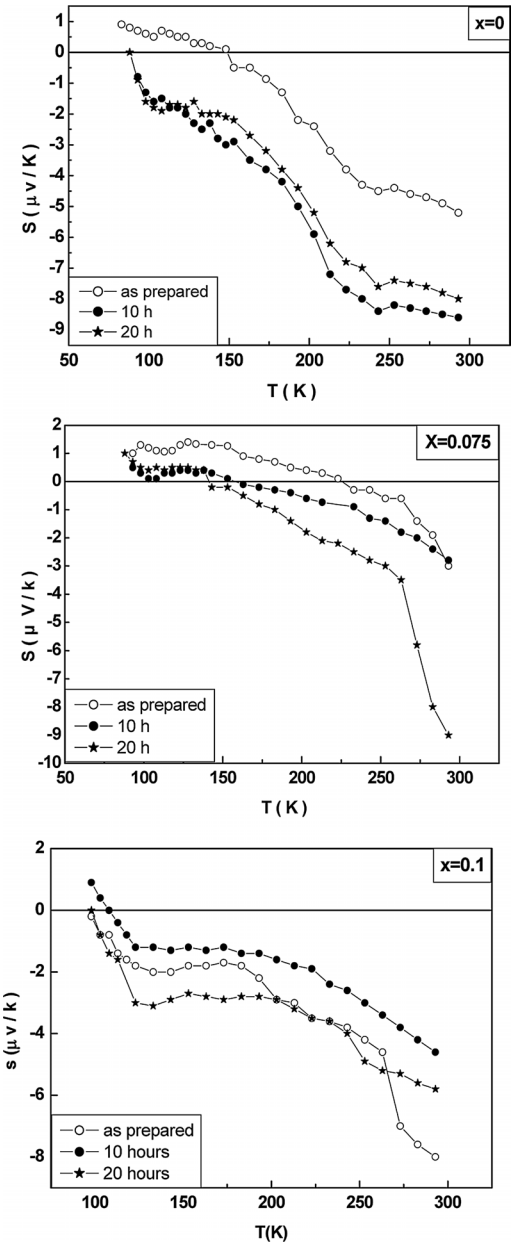

Figure 7 TEP of the as-prepared and annealed samples of $La_{0.7}Sr_{0.3}Mn_{1-x}Ni_xO_3$.

coefficient, and S_4 is the spin-wave fluctuation. Table 6 indicates that phonon and magnon drag coefficients have a little effect in this region, because of the small and nearly constant values that they have. As a whole, from this data, it is clear that diffusion and spin-wave fluctuation components have the most effective contribution below T_s. Data above T_s was analyzed by the Mott equation [35]:

$$S = k_B/e\,(E_s/k_BT + \alpha), \tag{10}$$

where E_s is the thermal activation energy, and α is a polaron kinetic-energy-related constant [43]. From Eq. (10), E_s seems to decrease with the first annealing time (10 h), and fluctuated with the second annealing time (20 h) (Table 7). In TEP, there are two important notes, the value of the α constant in Eq. (10) (Table 7) is less than unity (<1) and this confirms the small-polaron conduction in electrical measurements, and the value of E_s is less than $E\rho$, this large difference also supports the small polaron conduction at high temperature [35].

4 Conclusions Electrical resistivity, MR and TEP were studied as functions of annealing time. Resistivity increased with annealing times and there was a notable decrease in T_{ms}. An enhancement in MR with annealing time was also noticed in different temperature ranges for each sample, which was due to grain boundaries and oxygen vacancies. Moreover, the conduction mechanism above and below T_{ms} was examined. SPH and VRH models were used to examine the semiconducting region, SPH was dominant at $T > \theta_D/2$ and VRH at $T_{ms} < T < \theta_D/2$. The metallic region was examined by experimental relations, where the grain-boundary component was found to be the effective one. S was converted from positive to negative sign with annealing times at T^* and there was a general increase in the absolute value of S with annealing.

References

[1] I. El-Kassab, A. M. Ahmed, P. Mandal, K. Barner, A. Kattwinkel, and U. Sondermann, Phys. B **305**, 233 (2001).
[2] C. Zener, Phys. Rev. B **81**, 440 (1951).
[3] A. P. Ramirez, J. Phys.: Condens. Matter **9**, 8171 (1997).
[4] A. M. Ahmed, A. Kattwinkela, K. Barner, C. P. Yang, J. R. Sunb, and G. H. Rao, Phys. B **324**, 102 (2002).

Table 8 Values of S_0, S_1, $S_{3/2}$, S_3, and S_4 calculated below T_s in TEP.

x	conditions	S_0	S_1	$S_{3/2}$	S_3	S_4
0	as-prepared	−0.037	-5.8×10^{-4}	−0.499	0.249	-1.96×10^{-10}
	10 h	−8.06	−0.129	−0. 499	−0.250	-2.22×10^{-8}
	20 h	−23.43	−0.33	−0.500	0.249	-6.94×10^{-8}
0.075	as-prepared	−14.86	−0.2	−0.499	0.25	-2.14×10^{-8}
	10 h	−1.97	−0.0564	−0.499	0.25	-3.65×10^{-8}
	20 h	−31.08	−0.537	−0.499	0.25	-1.76×10^{-7}
0.1	as-prepared	13.52	−0.2118	−0.49	0.25	-3.099×10^{-9}
	10 h	1.7	-3.8×10^{-2}	−0.500	0.25	9×10^{-9}
	20 h	−17	0.16	−0.5	0.25	1.4×10^{-8}

[5] S. Tabatabai Yazdi, N. Tajabor, and D. S. Khoshnoud, J. Magn. Magn. Mater. **322**, 3131 (2010).
[6] N. Abdelmoula, J. Dhahri, K. Guidara, E. Dhahri, and J. C. Joubert, Phase Transit. **70**, 197 (1999).
[7] A. J. Millis, P. B. Littlewood, and B. I. Shraiman, Phys. Rev. Lett. **74**, 5144 (1995).
[8] I. Terasaki, Y. Sasago, and K. Uchinokura, Phys. Rev. B **56**, 12685 (1997).
[9] S. Hébert, D. Flahaut, C. Martin, S. Lemonnier, J. Noudem, C. Goupil, A. Maignan, and J. Hejtmanek, Prog. Solid State Chem. **35**, 457 (2007).
[10] V. L. Kozhevnikov, I. A. Leonidov, E. B. Mitberg, M. V. Patrakeev, Y. M. Baikov, V. S. Zakhvalinskii, and E. Lähderant, J. Solid State Chem. **172**, 1 (2003).
[11] G. Venkataiah, J. C. A. Huang, and P. V. Reddy, J. Alloys Compd. **562**, 128 (2013).
[12] G. B. Chon, H. S. Im, Sang M. Lee, B. H. Koo, C. G. Lee, and M. H. Jung, J. Magn. Magn. Mater. **310**, 927 (2007).
[13] T. L. Phan, Q. T. Tran, P. Q. Thanh, P. D. H. Yen, T. D. Thanh, and S. C. Yu, Solid State Commun. **184**, 40 (2014).
[14] H. Hwang, S.-W. Cheong, N. P. Ong, and B. Batlogg, Phys. Rev. Lett. **77**, 2041 (1996).
[15] R. V. Wandekar, B. N. Wani, and S. R. Bharadwaj, Solid State Sci. **11**, 240 (2009).
[16] S. Kuharuangrong, Ceram. Int. **30**, 273 (2004).
[17] K. Horiba, A. Chikamatsu, H. Kumigashira, M. Oshima, H. Wadati, A. Fujimori, M. Lippmaa, M. Kawasaki, and H. Koinuma, J. Electron. Spectrosc. Relat. Phenom. **156–158**, 375 (2007).
[18] A. M. Ahmed, A. K. Diab, and H. F. Mohamed, J. Supercond. Nov. Magn. **24**, 597 (2011).
[19] A. M. Ahmed, S. A. Saleh, E. M. M. Ibrahim, and H. F. Mohamed, J. Magn. Magn. Mater. **301**, 452 (2006).
[20] A. M. Ahmed, Phys. B **352**, 330 (2004).
[21] R. V. Wandekar, B. N. Wani, and S. R. Bharadwaj, Mater. Lett. **59**, 2799 (2005).
[22] A. M. Ahmed, S. A. Saleh, E. M. M. Ibrahim, E. Bontempi, and H. F. Mohamed, J. Magn. Magn. Mater. **320**, 43 (2008).
[23] C. V. Vazquez, M. C. Blanco, M. A. L. Quintela, R. D. Sanchez, J. Rivas, and S. B. Oseroff, J. Mater. Chem. **8**, 991 (1998).
[24] R. Mahesh, R. Mahendiran, A. K. Raychaudhuri, and C. N. R. Rao, Appl. Phys. Lett. **68**, 2291 (1996).
[25] M. Sugantha, R. S. Singh, A. Guha, A. K. Raychaudhuri, and C. N. R. Rao, Mater. Res. Bull. **33**, 1129 (1998).
[26] A. Nossov, J. Pierre, V. Vassiliev, and V. Ustinov, Solid State Commun. **101**, 361 (1997).
[27] A. K. M. A. Hossain, L. F. Cohen, T. Kodenkandeth, J. MacManus-Driscoll, and N. M. Alford, J. Magn. Magn. Mater. **195**, 31 (1999).
[28] S. Othmani, M. Bejar, E. Dhahri, and E. K. Hlil, J. Alloys Compd. **475**, 46 (2009).
[29] B. Roy, A. Poddar, and S. Das, J. Appl. Phys. **100**, 104318 (2006).
[30] P. Dey and T. K. Nath, Phys. Rev. B **73**, 214425 (2006).
[31] L. E. Hueso, J. Rivas, F. Rivadulla, M. A. Lopez-Quintela, and F. Rivadulla, J. Appl. Phys. **86**, 3881 (1999).
[32] J. Park, E. Vescovo, H. J. Kim, C. Kown, R. Ramesh, and T. Venkatesan, Phys. Rev. Lett. **81**, 1953 (1998).
[33] H. L. Ju, J. Gopalakrishnan, J. L. Peng, Q. Li, G. C. Xiong, T. Venkatesan, and R. L. Greene, Phys. Rev. B **5**, 6143 (1995).
[34] N. Abdelmoula, A. C. Rouhou, and L. Reversat, J. Phys.: Condens. Matter **13**, 449 (2001).
[35] N. F. Mott and E. A. Davis, 2nd edn. (Clarendon Press, Oxford, 2012)
[36] M. Jaime, M. B. Salamon, M. Rubenstein, R. E. Treece, J. S. Horwitz, and D. B. Chrisey, Phys. Rev. B **54**, 11914 (1996).
[37] I. G. Austin and N. F. Mott, Adv. Phys. **18**, 41 (1969).
[38] O. Raita, M. N. Grecu, X. Filip, D. Toloman, L. M. Giurgiu, S. Idziak, and S. K. Hoffmann, Acta Phys. Pol. A **108**, 113 (2005).
[39] T. Holstein, Ann. Phys. **8**, 343 (1959).
[40] S. Ravi and M. Kar, Phys. B **348**, 169 (2004).
[41] J. A. M. van Roosmalen, P. van Vlaanderen, and E. H. P. Cordfunke, J. Solid State Chem. **114**, 516 (1995).
[42] O. E. Ahlgren and F. W. Poulsen, Solid State Ion. **86–88**, 1173 (1996).
[43] K. Sega, Y. Kuroda, and H. Sakata, J. Mater. Sci. **33**, 1303 (1998).